Flow boiling heat transfer analysis of Al$_2$O$_3$ and TiO$_2$ nanofluids in horizontal tube using artificial neural network (ANN)

Manish Dadhich[1] · Om Shankar Prajapati[1] · Nirupam Rohatgi[2]

Abstract

A nanofluid is a suspension of nanometer-sized particles in a base fluid. In the last decade, flow boiling of nanofluid has gained much attention. However, only a few correlations on flow boiling are available. In this paper, an experimental study for HTC (heat transfer coefficient) of water-based TiO$_2$ and Al$_2$O$_3$ nanofluids flowing in an annulus has been carried out at 1 bar. The volumetric concentration of the nanofluid was varied from 0.05 to 0.20%, and heat flux and the mass flux were varied from 6.25 to 143.2 kW m^{-2} and 338 to 1014 kg m^{-2} s^{-1}, respectively. It was observed that HTC for both the nanofluids was greater than that of the base fluid water, and it increased with increase in the concentration of the nanoparticles, the heat flux and the mass flux. The highest HTC was obtained for Al$_2$O$_3$ nanofluid at 0.20% concentration for the heat flux of 143.2 kW m^{-2} and mass flux of 1014 kg m^{-2} s^{-1}. It was found that nanofluid made from Al$_2$O$_3$ nanoparticles had better HTC than nanofluid made from TiO$_2$ nanoparticles. The HTC ratios, i.e., the ratio of HTC of the nanofluid to the HTC of the base fluid, also increased with the increase in concentration, heat flux and mass flux. In the later part of the paper, new correlations were developed for predicting HTC for TiO$_2$ and Al$_2$O$_3$ nanofluids. Finally, an ANN model was developed to predict the heat transfer coefficient. Experimental values were found to be in good agreement with ANN predictions.

Keywords Nanofluids · Heat transfer coefficient · Mass flux · Heat flux · Concentration · Correlation · Artificial neural network

List of symbols

C	Concentration of nanofluids
C_p	Specific heat at constant pressure (J kg^{-1} K^{-1})
d_h	The hydraulic diameter of the tube m
F	Two-phase multiplier
h	Boiling heat transfer coefficient (kW m^{-2} K^{-1})
h_{LG}	Latent heat of vaporization (J kg^{-1})
k	Thermal conductivity (Wm^{-1} K^{-1})
$\dot{m}$	Total mass flux of the liquid and vapor flowing (kg m^{-2} s^{-1})
m	Mass of nanoparticle gm
M	Number of independent variables
Nu	Nusselt number
Pr	Prandtl number
Δp_{sat}	($p_{wall} - p_{sat}$) (Pa)
q	Heat flux (kW m^{-2})
δR	Uncertainties associated with the dependent variables
Re	Reynolds number
R^2	Correlation coefficient
S	Nucleate boiling suppression factor
ΔT_{sat}	($T_{wall} - T_{sat}$) (K)
x	Vapor quality
X_{tt}	Martinelli parameter
δX_j	Uncertainties associated with the independent variables

Greek symbols

α	Convective heat transfer coefficient (kW m^{-2} K^{-1})
μ	Dynamic viscosity (kg m^{-1} s^{-1})
ρ	Density (kg m^{-3})
σ	Surface tension (Nm^{-1})
ϕ	Nanoparticles volume concentration

✉ Manish Dadhich
   manish.ddh1988@gmail.com

[1] Department of Mechanical Engineering, University Teaching Department, Rajasthan Technical University, Kota, Rajasthan, India

[2] Department of Mechanical Engineering, Malaviya National Institute of Technology, Jaipur, Rajasthan, India

Subscripts

bf	Base fluid
cb	Convective boiling
FZ	Forster and Zuber
G	Gas phase
j	Specific parameter counter
L	Liquid phase
LG	Liquid–gas phase
nb	Nucleate boiling
np	Nanoparticle
sat	Saturated
tp	Two-phase

Abbreviations

ANN	Artificial neural network
CAD	Computer-aided design
CHF	Critical heat flux ($kW\ m^{-2}$)
DAQ	Data acquisition
DC	Direct current (ampere)
DI	Deionized
EPE	Expanded polyethylene
HDD	Hard disk drive
HTC	Heat transfer coefficient ($kW\ m^{-2}\ K^{-1}$)
MSE	Mean square error
ONB	Onset of nucleate boiling
RAM	Random access memory
SS	Stainless steel
UVM	Ultrasonic vibration machine

Introduction

Due to continuous depletion of energy resources and ever-growing problem of global warming, a lot of attention is being directed toward energy conservation and management. In many industrial applications, the efficiency of heat transfer equipment is of major concern. Many active and passive techniques are already in use to improve the heat transfer rate.

Water, ethylene glycol and oils are commonly used for the transfer of heat, but their efficiency is quite low. Therefore, researchers are working on different ways to improve the heat transfer efficiency of the fluids. nanofluids, i.e., nanoparticles suspended in the water, ethylene glycol and oils provide an attractive option for improving the efficiency of heat transfer systems. Nanoparticles have major effects on the thermo-physical properties like density, viscosity, specific heat and thermal conductivity of base fluids like water, oils, etc. The significant increase in the convective heat transfer coefficient is seen in flow boiling process by using nanoparticles in the base fluids. A very important role is played by boiling heat transfer in a number of industrial applications. The main applications

are fusion reactors, heat exchangers, steam generators, etc. Due to the importance of the boiling process, researchers are working on nanofluid flow boiling in pipes, annulus, etc., and extensively investigating it for horizontal and vertical flow conditions.

Azmi et al. [1] carried out an experimental study on TiO_2–water nanofluid flowing in a copper tube having volumetric concentration up to 3.0% to determine the heat transfer coefficient. During the investigation, the Reynolds number was varied from 8000 to 30,000 and tapes having different twist ratio were inserted in the tube. For the uniform heating of the copper tube, two nichrome heaters having 1.5 kW maximum electric rating were wrapped around the tube. Maximum enhancement in the heat transfer coefficient of TiO_2–water nanofluid was 81.1% at $Re = 23,558$, the concentration of 1.0% and the twist ratio of 5 in comparison with water flowing through the tube. As the concentration of nanofluid was increased to 3.0%, the heat transfer coefficient decreased and was lower than the base fluid water. Zhou et al. [2] experimentally investigated the performance of water-based Al_2O_3 nanofluid flowing through rectangular minichannels. During the investigation, mass flux and heat flux were varied from 80 to 350 $kg\ m^{-2}\ s^{-1}$ and 18 to 200 $kW\ m^{-2}$, respectively. Mass fraction of water–Al_2O_3 nanofluid was varied three times, i.e., 0.2%, 0.5% and 1.0%. Results revealed that with the addition of nanoparticles in the base fluid the heat transfer performance was enhanced. Heat transfer coefficient was enhanced by 11.2%, 15.4% and 18.7% for the mass fraction of 0.2 wt%, 0.5 wt% and 1.0 wt%, respectively, in comparison with water. Using Al_2O_3 nanofluids, Kim et al. [3] carried out flow boiling experiments in the vertical tube at a lower flow rate and pressure to study the effect on CHF. The results indicated up to 70% increment in CHF by using nanofluids. A comparison was made between deionized water and nanofluids of alumina particle by Ahn et al. [4] having 0.01% volumetric fraction and 47 nm average diameter of the nanoparticle. An increment of 40% with respect to the base fluid water was observed in CHF when nanofluid was flowing with a velocity of 4 $m\ s^{-1}$.

An experimental study was carried out by Kahani et al. [5] with Al_2O_3–water and TiO_2–water nanofluids. Nanofluids were made to flow through helically coiled tubes at constant heat flux. It was observed that Al_2O_3–water nanofluid had better heat transfer performance than TiO_2–water nanofluid because of higher thermal conductivity and smaller size of Al_2O_3 nanoparticles. Karimzadehkhouei et al. [6] conducted flow boiling experiments on horizontal smooth microtubes. Al_2O_3–water and TiO_2–water nanofluids were used as working fluids. It was observed that at lower Reynolds numbers there was no significant improvement in heat transfer but as the

Reynolds numbers increased significant improvement in heat transfer was observed. Kim et al. [7] conducted experiments on a vertical stainless steel test section having a length of 100 mm, the outer diameter of 6.35 mm and a thickness of 0.41 mm. Water-based diamond, zinc oxide and alumina nanofluids having volumetric concentration lower than 0.1% were used for the experiments. The results showed that for subcooled flow boiling, nanofluids heat transfer coefficient was 20% higher than that for the base fluid water.

Kim et al. [8] carried out flow boiling experiments in a tube having Al$_2$O$_3$ nanoparticle deposition to study the effect of deposition on CHF. An enhancement of about 80% was observed in flow boiling CHF for a tube having deposits of Al$_2$O$_3$ nanoparticles than the simple tube. Abedini et al. [9] carried out nanofluid flow boiling experiments in horizontal as well as vertical tubes using water/TiO$_2$ nanofluid. It was observed that with the increase in TiO$_2$ nanoparticles concentration, the heat transfer coefficient of nanofluid decreased for both the tubes. But vapor volume fraction was increased with the addition of nanoparticle in the base fluid. Hasheminia et al. [10] numerically examined the effects of concentration of nanoparticles and temperature profile on critical heat flux (CHF). Results showed that as the volume fraction of nanoparticles increased there was a noticeable decrease in CHF for Al$_2$O$_3$/water and SiO$_2$/water nanofluids. The reason for the decrease in CHF was increase in the surface contact angle. By utilizing water/ZnO nanofluid, Prajapati and Rohatgi [11] analyzed enhancement in the heat transfer during flow boiling. ZnO nanoparticle concentration was changed from 0.0001 to 0.1 vol.% in the base fluid. A 126% enhancement was seen in the heat transfer coefficient in comparison with that of the base fluid.

Zeitoun and Ali [12] carried out an experimental investigation to examine the heat transfer effect between the vertical alumina–water nanofluid jet and a horizontal circular round surface. During the examination, nanoparticle concentration was changed to 0, 6.6 and 10%, in the base fluid water. The flow rate of jet, the diameter of the disk and the diameter of the jet nozzle were also changed during the investigation. Results indicated that the heat transfer process was enhanced as nanofluid acted as a good heat carrier. At constant Reynolds number, increase in the Nusselt numbers was observed with the increase in nanoparticle concentration. Qi et al. [13] numerically and experimentally investigated heat transfer characteristics of water–TiO$_2$ nanofluids and DI water in circular and corrugated stainless steel tubes. Comparison of results of DI water and TiO$_2$–water nanofluid showed that the combination of water–TiO$_2$ nanofluid and corrugated tube was better than other combinations by 53.95%.

Abdollahi et al. [14] numerically studied the fluid behavior and heat transfer characteristics of nanofluid flowing in microchannel heat sink having V-type inlet and outlet arrangement. Four working nanofluids, Al$_2$O$_3$, SiO$_2$, ZnO and CuO nanoparticles, having volume fractions of 1%, 1.5% and 2%, were taken for analysis. Pure water was used as a base fluid. The diameters of the nanoparticles were 30 nm, 40 nm and 60 nm. The study showed that SiO$_2$ nanofluid with 30 nm nanoparticle diameter and 2% volume fraction was having a higher heat transfer rate than all other nanofluids. Wang and Su [15] carried out flow boiling experiments in a vertical tube to study the heat transfer characteristics of γ-Al$_2$O$_3$/H$_2$O nanofluids. Average particle diameter was 20 nm, and the volume concentrations were taken as 0.1% and 0.5%. The experiments were performed for surface heat flux 50–300 kW m^{-2}, mass flux 350–1100 kg m^{-2} s^{-1} and pressure 0.2–0.8 MPa. Results showed 86% enhancement in heat transfer for γ-Al$_2$O$_3$/H$_2$O nanofluids with respect to pure water. Increase in Nusselt number during flow boiling was observed with the increase in surface heat flux, pressure and nanoparticles volume concentration. For volume concentration 0.1% and 0.5%, increase in Nusselt number was 23% and 45%, respectively.

Mohammed et al. [16] carried out experimental work on flow boiling at operating conditions similar to the conditions that are found in the vapor absorption refrigeration system. The fluid used during the investigation was nano-salt fluid with acetone/ZnBr$_2$ as the base fluid and graphene as nanoparticles. The investigation was carried out on nanoparticle concentration, boiler temperature and flow rate. Results showed that the Rohsenow constant in the correlation of flow boiling using nanofluid acetone/ZnBr$_2$ with graphene on the surface of stainless steel was 0.217. When the particle concentration was increased from 0 to 0.5 vol.%, the heat flux, as well as HTC on a heated surface, increased from 8638 Wm^{-2} and 106 W m^{-2} K^{-1} to 13,164 W m^{-2} and 167 W m^{-2} K^{-1}, respectively. Sarafraz et al. [17] performed an experiment to examine the flow boiling heat transfer characteristics of MgO/therminol 66 nanofluid which was used as a coolant on a disk made up of copper. Flow boiling HTC was increased with the presence of MgO/therminol 66 as compared to the base fluid. However, HTC decreased with the increase in mass concentration. Maximum enhancement in HTC was noticed at 0.1 wt%. The increase in HTC was 23.7%, 16.2% and 13.3% for 0.1 wt%, 0.2 wt% and 0.3 wt%, respectively.

Moreira et al. [18] carried out an experimental examination to study the effect of nanoparticle addition to water on HTC during flow boiling in a tube having an internal diameter of 1.1 mm. Nanoparticles used were Al$_2$O$_3$ and SiO$_2$ having volumetric concentrations 0.001%, 0.01% and

0.1%. Heat flux was varied up to 350 kW m^{-2}, and mass flux was varied from 200 to 600 kg m^{-2} s^{-1}. Results showed that the boiling HTC of nanofluid was lower than water in a tube without nanoparticles deposition. The behavior of heat transfer was affected by the dimension of nanoparticles. As this was related to deposition of nanoparticles on the surface and its impact on active nucleate site density, it was concluded that the size of nanoparticles plays a major role in deposition characteristics. Kamel et al. [19] carried out a review of nanofluid boiling experimental studies. Their focus was on the influence of parameters which were related to the operating conditions and morphology of nanoparticles on HTC and critical heat flux. Table 1 shows the previous experimental studies on flow boiling heat transfer coefficient of nanofluids.

The objective of the present study is to investigate and identify the parameters which affect the heat transfer coefficient during two-phase flow boiling process in a horizontal annulus. The experiments were performed for two different nanofluids (Al$_2$O$_3$–water and TiO$_2$–water), having volumetric concentrations of 0.05%, 0.1%, 0.15% and 0.20%. Mass flux and heat flux were varied while pressure was kept constant at 1 bar during the experiments. Experiments were performed for pure DI water, Al$_2$O$_3$–water nanofluid and TiO$_2$–water nanofluid in flow boiling. The results of DI water were compared with Al$_2$O$_3$–water and TiO$_2$–water nanofluids. The experimentally calculated heat transfer coefficient of DI water was validated with a leading predictive correlation of Chen [29]. The heat transfer coefficient of DI water and nanofluids with different volume concentrations and operating conditions was evaluated to study the effects of thermo-physical properties on flow and heat transfer.

The heat flux was varied in the range of (6.25–143.23) kW m^{-2}, and the mass flux was varied in the range of (338.13–1014.40) kg m^{-2} s^{-1}. Water was taken as the base fluid, and two nanofluids of Al$_2$O$_3$ and TiO$_2$ nanoparticles having a volumetric concentration (0.05–0.20%) were used in the experiments. Al$_2$O$_3$ and TiO$_2$ nanofluids were used for the study as they are widely used in many industrial applications. Power-law-based HTC correlation was developed for both the nanofluids. An ANN model was also developed to predict HTC.

Nanofluid preparation

When nanometer-sized particles are dispersed into the base fluid like water, ethylene glycol, oil, etc., and mixed with the base fluid, the fluid formed is called nanofluid. It is a colloidal suspension of nanoparticles in a base fluid. The base fluid used in the current study is deionized water and at 1 bar the boiling point of the base fluid is 100 °C. Nanoparticles are made up of carbides, oxides, metals or carbon nanotubes. Properties of the nanoparticles used in the experiments, i.e., Al$_2$O$_3$ and TiO$_2$, are given in Table 2.

For the experiments on nanofluids, preparation of nanofluid is a very important step because if the nanofluid is not prepared in a proper way then the agglomeration of

Table 1 Previous studies on flow boiling heat transfer coefficient of nanofluids

Authors	Nanofluids type	Concentration (C) of nanofluid	Size of particle/nm	Impact on heat transfer coefficient
Sarafraz and Hormozi [20]	Water with CuO	0.5–1.5% by volume %	50	No noticeable effect was noticed
Rana et al. [21]	Water with ZnO	0.001–0.01% by volume %	40	Increment in the heat transfer coefficient was noticed
Edel and Mukherjee [22]	Water with Al$_2$O$_3$	0.001 by volume %	20–40	Increment in the heat transfer coefficient was noticed
Moreira et al. [23]	Water with Al$_2$O$_3$	0.001–0.1% by volume %	20–30	No noticeable effect was noticed
Duursma et al. [24]	Ethanol with Al$_2$O$_3$	0.01 to 0.1 by volume %	< 50	Increment by 400% in the heat transfer coefficient was noticed at a concentration of 5×10^{-2} by volume %
Xu and Xu [25]	Water with Al$_2$O$_3$	0.052% by volume %	40	Increment in the heat transfer coefficient was noticed
Chehade et al. [26]	Water with Ag	2.37×10^{-4} to 4.75×10^{-4} by volume %	35	Increment by 132 to 162% in heat transfer coefficient was noticed
Sarafraz and Hormozi [27]	Water with Al$_2$O$_3$	0.5–1.5% by volume %	50	Increment in the heat transfer coefficient was noticed at lower heat fluxes and no noticeable effect was noticed at higher heat fluxes
Paul et al. [28]	Al$_2$O$_3$ with water	0.1% and 0.3% by volume %	26	Increment in the heat transfer coefficient was noticed

Table 2 Physical properties of metal oxide nanomaterials

Nanoparticles	Density/ kg m^{-3}	Specific surface area/m^2 g^{-1}	Average particle size/nm	Particle shape	Thermal conductivity/Wm^{-1} K^{-1}
Al$_2$O$_3$	3880	60	40	Spherical	36
TiO$_2$	4175	50	30	Spherical	8.4

Table 3 Thermo-physical properties of nanofluids at various concentrations based on deionized water

Nanofluids	Volumetric concentration/%	Density/ kg m^{-3}	Specific heat capacity/ J kg^{-1} K^{-1}	Thermal conductivity/ Wm^{-1} K^{-1}	Dynamic viscosity/ kg m^{-1} s^{-1}
Deionized water	0	970.86	4197	0.67	0.00039
Al$_2$O$_3$	0.05	972.31	4190	1.05	0.00042
	0.10	973.76	4183	1.12	0.00045
	0.15	975.22	4176	1.18	0.00048
	0.20	976.67	4169	1.25	0.00051
TiO$_2$	0.05	972.46	4189	0.81	0.00053
	0.10	974.05	4182	0.84	0.00056
	0.15	975.66	4174	0.87	0.00059
	0.20	977.22	4167	0.90	0.00062

nanoparticles may occur during the experiments. Proper mixing gives stability to the nanofluids. Two-step technique was used to prepare nanofluids. An ultrasonic vibration machine (UVM) was used to disperse nanoparticles into the base fluid, i.e., water. Mixing time depends on the nanoparticle used and its concentration. Sonication time for Al$_2$O$_3$ was 6–7 h and that for TiO$_2$ was 4–5 h. After sonication stability of the nanofluids is checked by visual inspection. Mass of the nanoparticles required in the base fluid for different concentrations of nanofluids is calculated using the following equation [30]:

$$m_{\mathrm{np}} = \left(\frac{\emptyset}{100 - \emptyset}\right)\left(\frac{\rho_{\mathrm{np}}}{\rho_{\mathrm{bf}}}\right)m_{\mathrm{bf}} \qquad (1)$$

where m_{np} = mass of nanoparticle, m_{bf} = mass of base fluid, $\emptyset$ = volumetric concentration, ρ_{np} = density of nanoparticle and ρ_{bf} = density of base fluid.

Properties of nanofluids at different concentrations and at temperature 80 °C were measured. Thermo-physical properties of nanofluids at various concentrations based on deionized water are given in Table 3.

Flow boiling experimental setup

Schematic diagram of the experimental setup is shown in Fig. 1. It is a closed-loop system consisting of a storage reservoir of 10-liter capacity, circulating pump, flowmeter,

horizontal annular test section which is electrically heated, condenser and heat exchanger. The fluid being studied is stored in the reservoir and pumped into the test section with the help of the circulating pump. The flow is controlled by different valves; a flowmeter is used to measure the flow rate. In the test section, the working fluid is boiled using electrically heated rod made of stainless steel. (Stainless steel is chosen as rod material because of its wide applications in industries). The mixture of liquid and steam is passed into the condenser and the heat exchanger before returning to the reservoir. The complete pipe sections and test section are thermally insulated by expanded polyethylene (EPE) foam in order to minimize the heat losses from the working fluid to the surroundings. The thickness of EPE foam is 1/2″ and thermal conductivity is 0.01 W m^{-1} K^{-1}. Electric power is supplied through a 64-kVA transformer. Copper rods, bus bars and shunt are used to supply DC. There are three loops in the experimental setup. Nanofluids flow in a closed primary loop. Cooling water flows in secondary open loop for condenser and heat exchanger and in tertiary open-loop cooling water flows to cool the transformer. The 3D CAD diagram of the experimental setup is shown in Fig. 2.

The test section

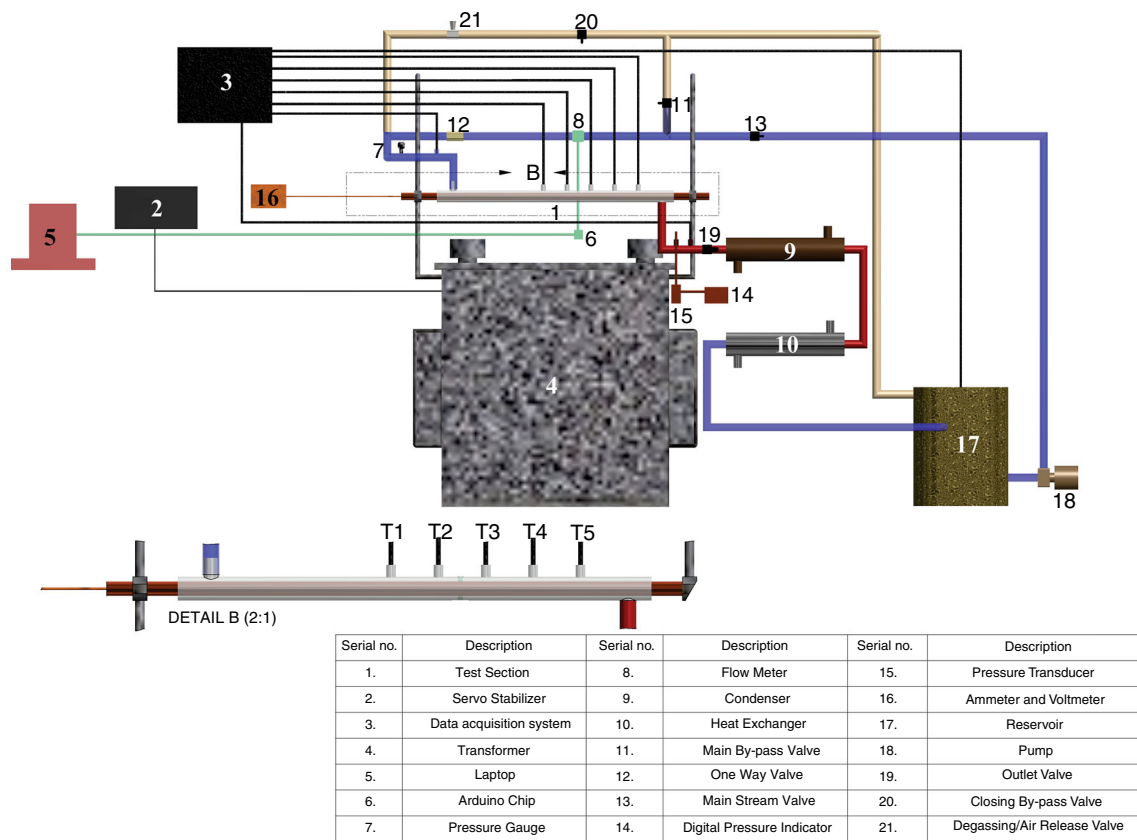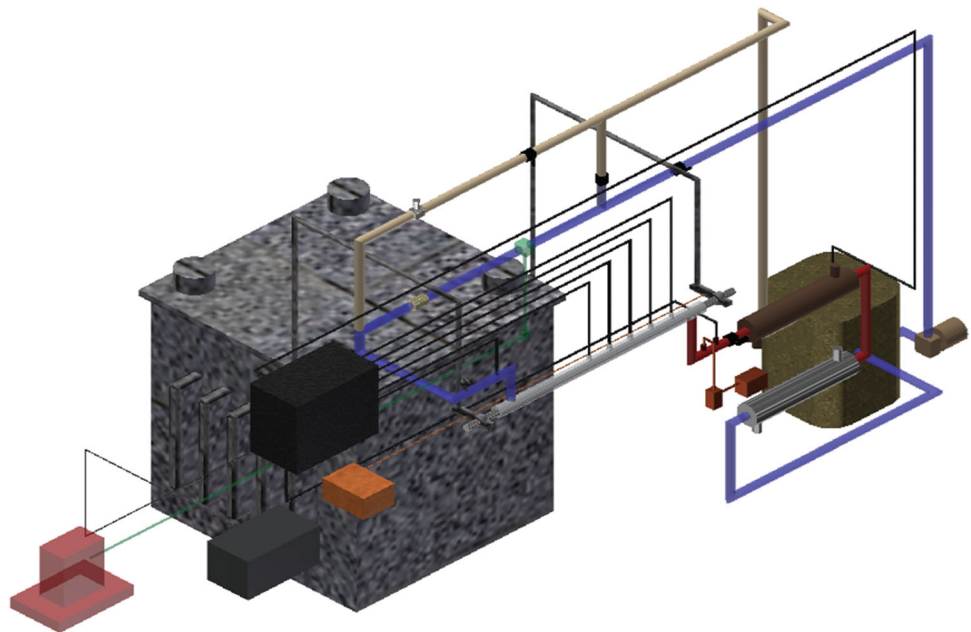The length of the test section is 780 mm. It was built on a concrete foundation. Working fluid flows through the

Fig. 1 Schematic diagram of the experimental setup

Serial no.	Description	Serial no.	Description	Serial no.	Description
1.	Test Section	8.	Flow Meter	15.	Pressure Transducer
2.	Servo Stabilizer	9.	Condenser	16.	Ammeter and Voltmeter
3.	Data acquisition system	10.	Heat Exchanger	17.	Reservoir
4.	Transformer	11.	Main By-pass Valve	18.	Pump
5.	Laptop	12.	One Way Valve	19.	Outlet Valve
6.	Arduino Chip	13.	Main Stream Valve	20.	Closing By-pass Valve
7.	Pressure Gauge	14.	Digital Pressure Indicator	21.	Degassing/Air Release Valve

Fig. 2 3D diagram of the experimental setup

annulus having an electrically heated rod of stainless steel inside a borosilicate glass tube. Copper rods are attached at both the ends of the SS rod to complete the circuit. The

heated section is 500 mm long. The inner diameter of the glass tube and the outer diameter of the rod are 21.8 and 12.7 mm, respectively. The schematic diagram of the test
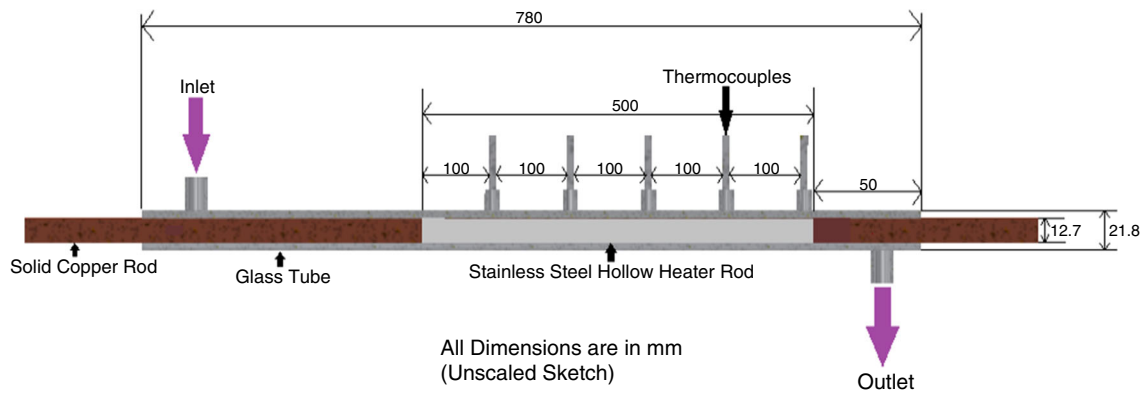
Fig. 3 Schematic diagram of the test section
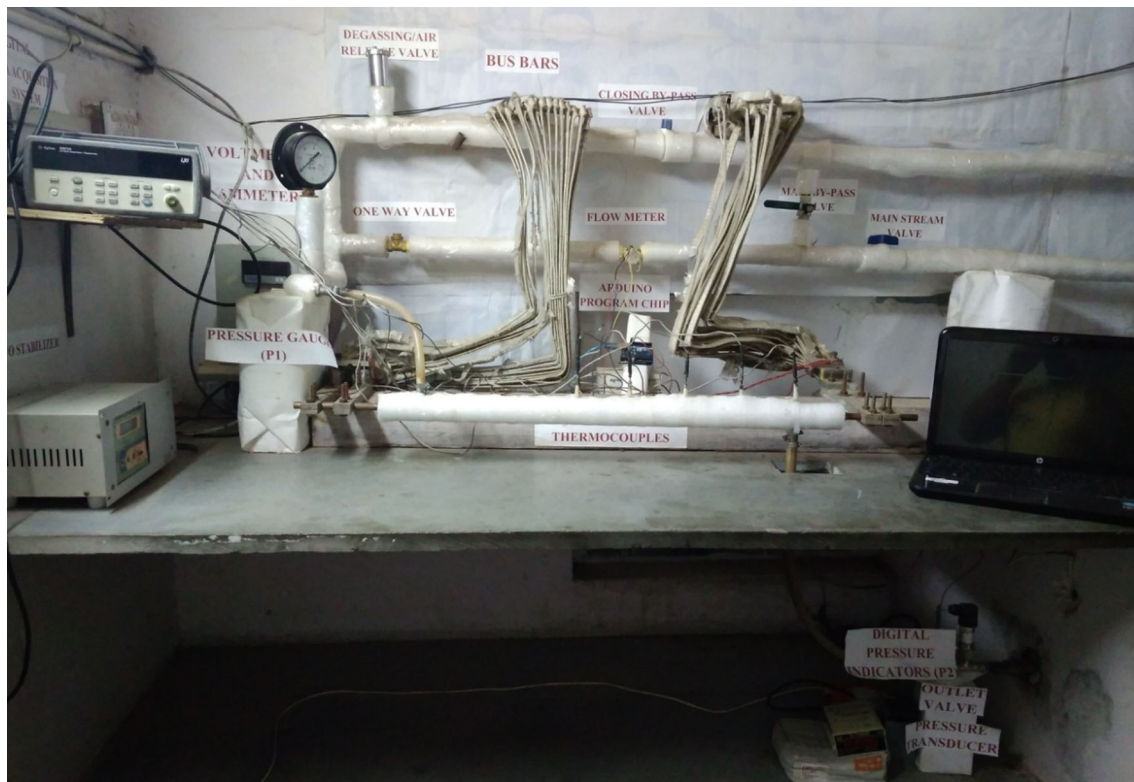
Fig. 4 Actual experimental setup

section is shown in Fig. 3, and the actual experimental setup is shown in Fig. 4.

The test section consists of a stainless steel pipe, solid copper rod, Teflon cork and borosilicate glass tube. Stainless steel pipe (grade SS310) has a length of 500 mm, the outer diameter of 12.7 mm and thickness of 1 mm. Two copper rods (diameter 12.7 mm) were attached to SS pipe at the inlet and the outlet for support and to complete the electric circuit. Five J-type thermocouples were placed inside the borosilicate glass tube. Teflon cork was fixed at both the ends of the tube and sealed with the adhesive paste in order to avoid any leakage. Finally, the section was covered with expanded polyethylene (EPE) to minimize the heat loss to the surrounding.

A heat exchanger was installed between the condenser and SS storage reservoir to cool the working fluid. Steam from the mixture of steam and fluid was condensed in the condenser. Both the heat exchanger and the condenser were made of stainless steel tubes.

Experimental

At the beginning of the experiments, the heating surface and the test section were cleaned. Deionized water and

Table 4 Parameter range during the experiments

S. no.	Parameter	Range
1	Concentration/%	0.05, 0.1, 0.15 and 0.20
2	Pressure/bar	1
3	Heat flux/kW m^{-2}	6.25–143.2
4	Sonication time/h	0–8
5	Average nanoparticle size/nm	40
6	Nanoparticles	Al_2O_3 and TiO_2
7	Mass flux/kg m^{-2} s^{-1}	338–1014
8	Inlet temperature/°C	80

Table 5 Uncertainty of physical quantities

S. no.	Variables	Uncertainty/%
1	Heat flux	3.23
2	Heat transfer coefficient	3.35
3	Mass flux	2.68

nanofluids were stored in the reservoir and maintained at a temperature of 80 °C. The temperature of the working fluid in the reservoir was maintained at 80 °C with the help of an electrical heater. The working fluid was pumped into the test section at the desired flow rate by a centrifugal pump. The flow rate of the working fluid was controlled with the help of valves. In the closed primary loop, working fluid was circulated at the desired pressure. Working fluid was boiled in the test section by the heater rod, and the required amount of voltage was supplied by the transformer. A mixture of steam and fluid was passed through the condenser and the heat exchanger to the reservoir. To avoid any sort of gas entrapment, degassing of working fluid was done before starting the experiment using degassing valve (Zoloto Valves). After the steady-state was reached, DAQ (data acquisition) system was used to record the readings. Every experiment was repeated three times to verify the readings. Above-mentioned process was repeated for every heat flux, concentration, working fluid and mass flow rate. Parameter's range used during the experiments is shown in Table 4.

Instruments used

Thermal property analyzer (KS-1 Sensor, KD2 Pro, accuracy ± 5%, Decagon Devices Inc.) was used to measure the thermal conductivity of water and nanofluids at different concentrations. DV-III ultra viscometer (accuracy ± 1%, Brookfield Engineering Laboratories, Inc.) was used to measure the viscosity of water and nanofluids at different concentrations. Hydrometer (accuracy ± 1 scale divisions) was used to measure the density of the water and nanofluids at different concentrations. Differential scanning calorimeter Q2000 (accuracy ± 1%, TA Instruments) was used to measure the specific heat of water and nanofluids at different concentrations. Flowmeter (YF-S201, accuracy ± 10%) was used to measure the mass flow rate of the working fluid. The flowmeter was attached to the ARDUINO chip, which converts analog data into

digital form. A laptop (hp g6-2004tx, Core i-5, 500 GB HDD and 8 GB RAM) was used to run the ARDUINO code which shows the values of mass flow rate. J-type thermocouples (JMQSS-IM050U-300, accuracy ± 0.1%, Omega Engineering Inc.) were used to measure inlet and outlet temperature of the working fluid and surface temperature at five locations in the test section. Temperatures were recorded by a data acquisition system (34972A LXI, Agilent Keysight Technologies). The pressure at the inlet of the test section was measured by a pressure gauge (accuracy ± 1%, H-Guru Industries), and pressure at the outlet of the test section was measured by a pressure transducer (accuracy ± 1%, Keller). The voltage across the heater rod and current through the heater rod were measured by voltmeter and ammeter (accuracy ± 1%, Meco Instruments Pvt. Ltd.).

Uncertainty analysis

Uncertainty analysis was performed to measure the error in the measurement of physical quantities using the standard uncertainty analysis equation [31].
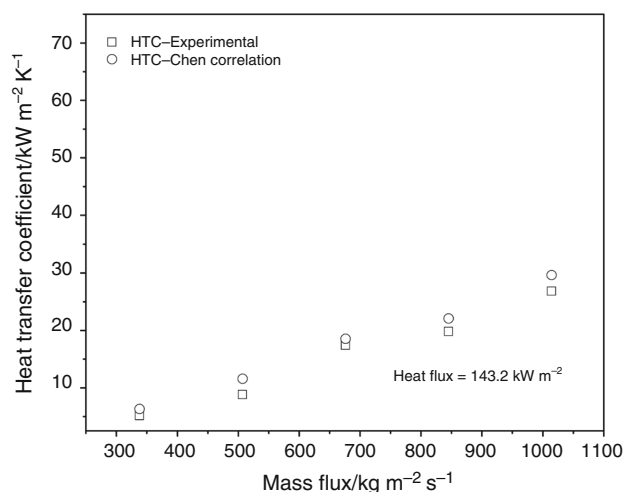

Fig. 5 Comparison between heat transfer coefficient of DI water obtained experimentally and by Chen correlation with mass flux at a constant heat flux of 143.2 kW m^{-2}
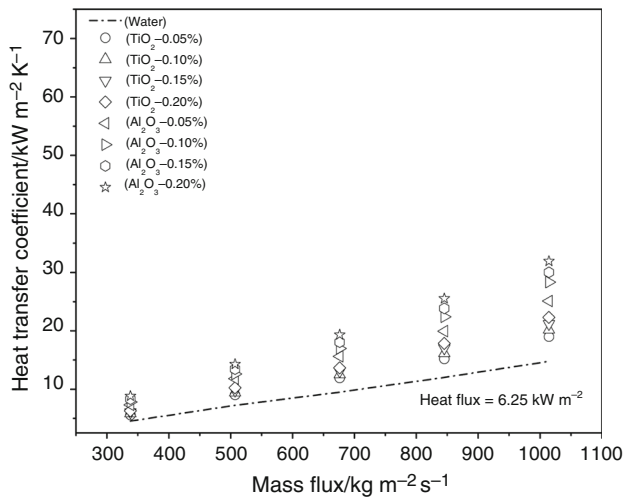
Fig. 6 Heat transfer coefficient of water, Al$_2$O$_3$ and TiO$_2$ nanofluids with mass flux at a heat flux of 6.25 kW m^{-2}
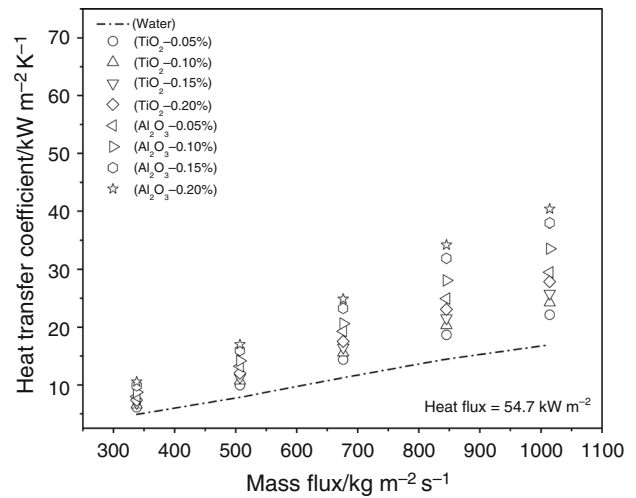
Fig. 8 Heat transfer coefficient of water, Al$_2$O$_3$ and TiO$_2$ nanofluids with mass flux at a heat flux of 54.7 kW m^{-2}
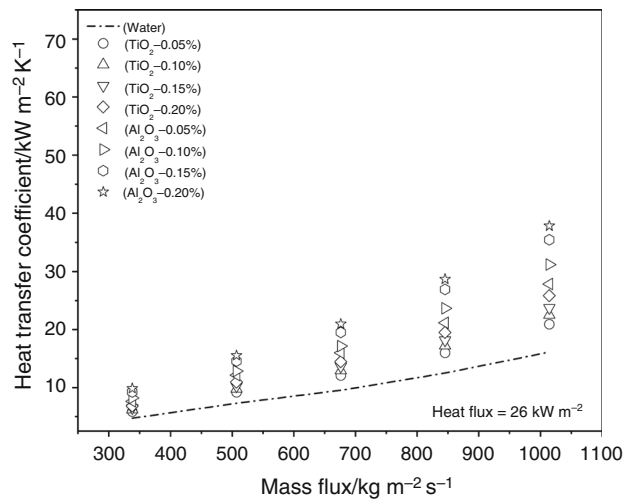
Fig. 7 Heat transfer coefficient of water, Al$_2$O$_3$ and TiO$_2$ nanofluids with mass flux at a heat flux of 26 kW m^{-2}
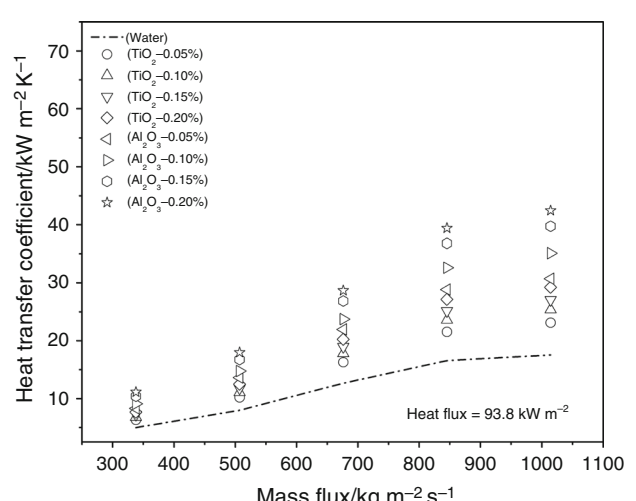
Fig. 9 Heat transfer coefficient of water, Al$_2$O$_3$ and TiO$_2$ nanofluids with mass flux at a heat flux of 93.8 kW m^{-2}

$$\delta R = \left[\sum_{j=1}^{M} \left(\frac{\partial R}{\partial X_j} \delta X_j \right)^2 \right]^{\frac{1}{2}} \qquad (2)$$

where j, M, δR and δX_j are the specific parameter counter, number of the independent variables, uncertainties associated with the dependent R and independent X_j variables.

Accordingly, uncertainties in the measurement of heat flux, heat transfer coefficient and mass flux were determined. Table 5 shows the uncertainty values for the above-mentioned quantities.

Experimental validation with Chen correlation

For establishing the integrity of the experimental setup, the values of heat transfer coefficients for DI water obtained experimentally at the highest heat flux of 143 kW m^{-2} and pressure of 1 bar were compared with the values obtained by Chen correlation.

The two-phase flow boiling heat transfer coefficient is the sum of the heat transfer coefficients for nucleate boiling and convective boiling. That is:

$$\alpha_{tp} = \alpha_{nb} + \alpha_{cb} \qquad (3)$$

Equation (3) was further modified as:

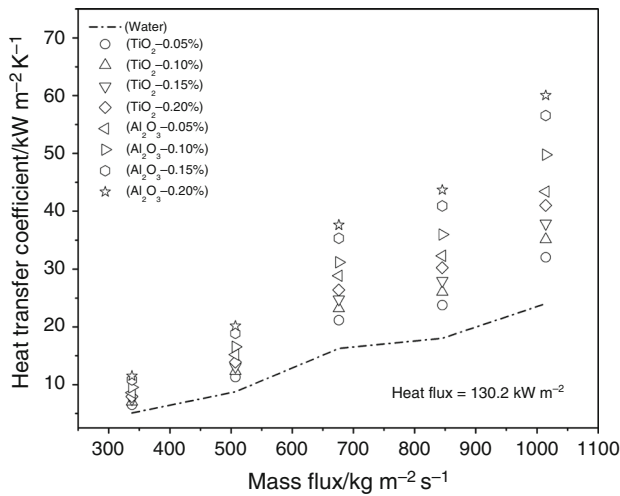$$\alpha_{tp} = \alpha_{FZ} S + \alpha_L F \qquad (4)$$

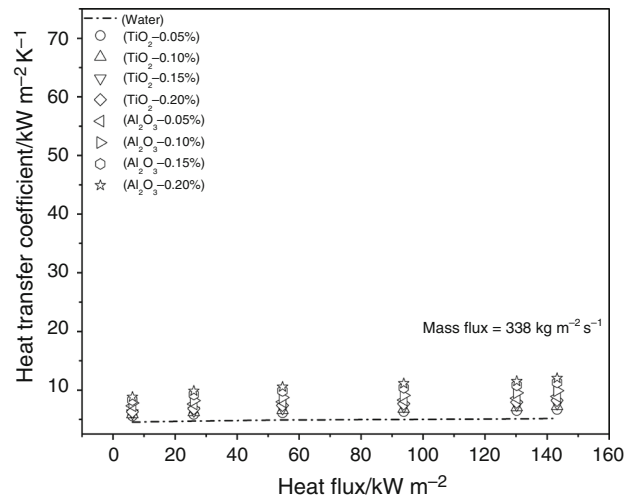**Fig. 10** Heat transfer coefficient of water, Al_2O_3 and TiO_2 nanofluids with mass flux at a heat flux of 130.2 kW m^{-2}

Fig. 12 Heat transfer coefficient of water, Al_2O_3 and TiO_2 nanofluids with heat flux at a mass flux of 338 kg m^{-2} s^{-1}
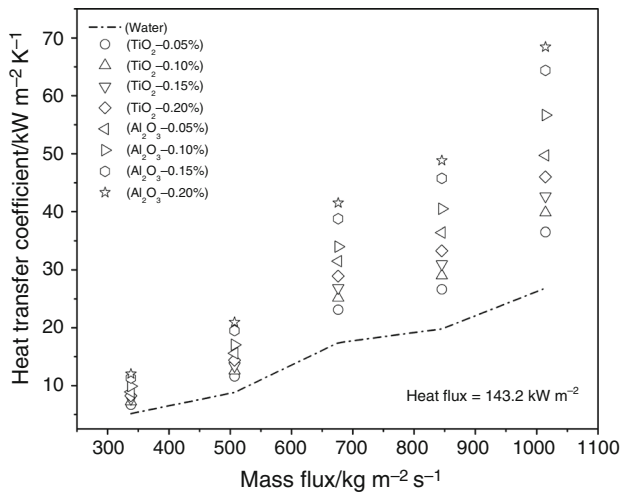

Fig. 11 Heat transfer coefficient of water, Al_2O_3 and TiO_2 nanofluids with mass flux at a heat flux of 143.2 kW m^{-2}
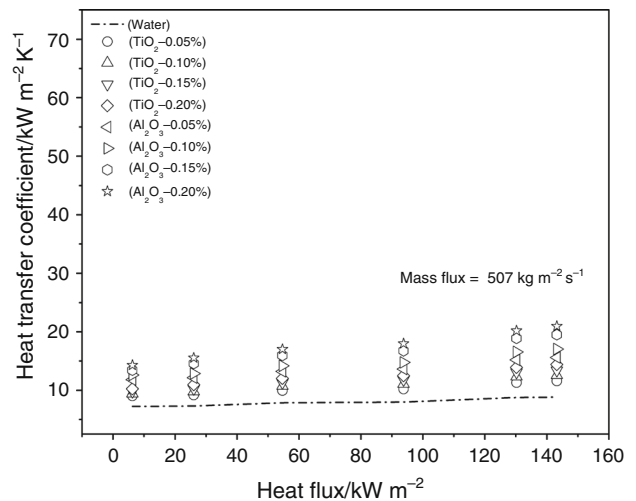
Fig. 13 Heat transfer coefficient of water, Al_2O_3 and TiO_2 nanofluids with heat flux at a mass flux of 507 kg m^{-2} s^{-1}

α_{FZ} = nucleate boiling heat transfer coefficient calculated by Forster and Zuber's nucleate pool boiling correlation, S = nucleate boiling suppression factor acting on α_{FZ}, α_L = liquid-phase convective heat transfer coefficient calculated by Dittus–Boelter turbulent flow correlation, F = two-phase multiplier which gives an increase in liquid-phase convection due to two-phase flow.

Nucleate pool boiling coefficient is calculated by Forster and Zuber correlation, i.e.,

$$\alpha_{FZ} = 0.00122 \left[\frac{k_L^{0.79} C_{pL}^{0.45} \rho_L^{0.49}}{\sigma^{0.5} \mu_L^{0.29} h_{LG}^{0.24} \rho_G^{0.24}} \right] \Delta T_{sat}^{0.24} \Delta p_{sat}^{0.75} \quad (5)$$

k_L = thermal conductivity of liquid water, C_{pL} = specific heat of liquid water, ρ_L = density of liquid water,

σ = surface tension of liquid water, μ_L = dynamic viscosity of liquid water, h_{LG} = latent heat of vaporization of liquid water, ρ_G = density of water vapor, $\Delta T_{sat} = (T_{wall} - T_{sat})$, difference between wall temperature of the rod and local saturation temperature, $\Delta p_{sat} = (p_{wall} - p_{sat})$, difference between the vapor pressure of the fluid at wall temperature of the rod and vapor pressure of the fluid at the local saturation temperature.

Using the Dittus–Boelter correlation, liquid-phase convective heat transfer coefficient is calculated:

$$\alpha_L = 0.023 \, Re_L^{0.8} Pr_L^{0.4} \left(\frac{k_l}{d_h} \right) \quad (6)$$
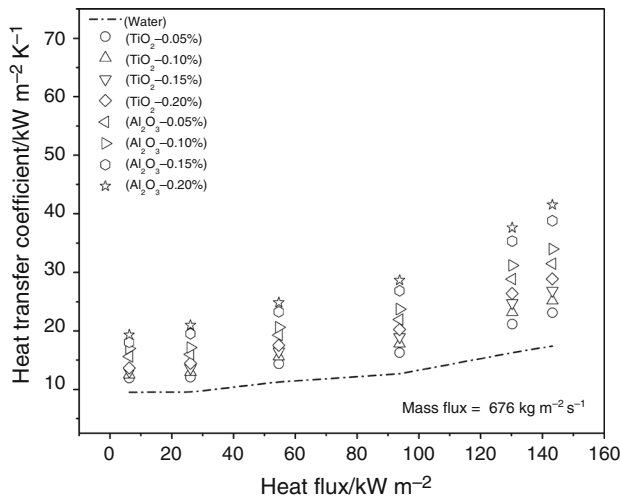
where the liquid Reynolds number is:

Fig. 14 Heat transfer coefficient of water, Al$_2$O$_3$ and TiO$_2$ nanofluids with heat flux at a mass flux of 676 kg m^{-2} s^{-1}
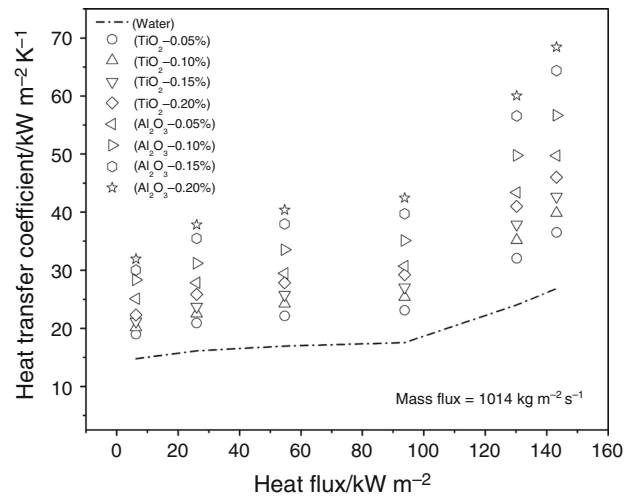

Fig. 16 Heat transfer coefficient of water, Al$_2$O$_3$ and TiO$_2$ nanofluids with heat flux at a mass flux of 1014 kg m^{-2} s^{-1}
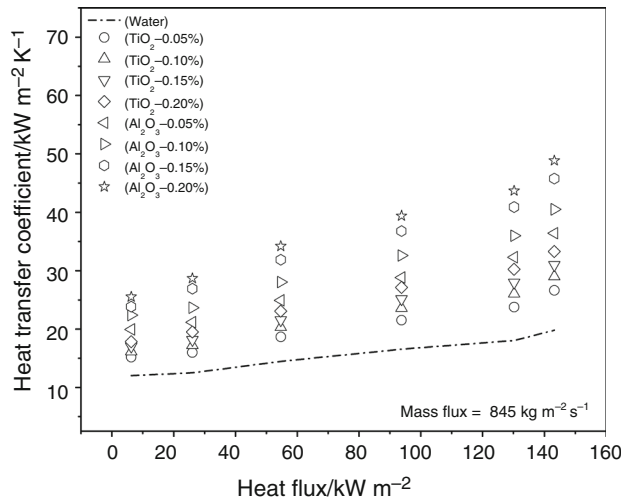
Fig. 15 Heat transfer coefficient of water, Al$_2$O$_3$ and TiO$_2$ nanofluids with heat flux at a mass flux of 845 kg m^{-2} s^{-1}
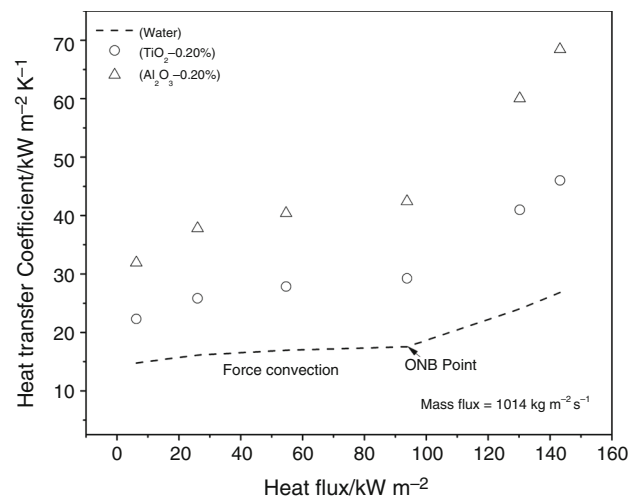

Fig. 17 Effect of heat flux on HTC of water and Al$_2$O$_3$ and TiO$_2$ nanofluids in forced convection and nucleate boiling region

$$Re_{\mathrm{L}} = \frac{\dot{m}(1-x)d_{\mathrm{h}}}{\mu_{\mathrm{L}}} \tag{7}$$

x = vapor quality, $\dot{m}$ = total mass flux of the liquid and vapor flow, d_{h}= hydraulic diameter of the tube through which fluid flows.

Liquid Prandtl number is given by:

$$Pr_{\mathrm{L}} = \frac{C_{\mathrm{pL}}\mu_{\mathrm{L}}}{k_{\mathrm{L}}} \tag{8}$$

The two-phase multiplier of Chen is given by:

$$F = \left(\frac{1}{X_{\mathrm{tt}}} + 0.213\right)^{0.736} \tag{9}$$

X_{tt} = Martinelli parameter used for the effect of two-phase-on convection is defined as:

$$X_{\mathrm{tt}} = \left(\frac{1-x}{x}\right)^{0.9}\left(\frac{\rho_{\mathrm{G}}}{\rho_{\mathrm{L}}}\right)^{0.5}\left(\frac{\mu_{\mathrm{L}}}{\mu_{\mathrm{G}}}\right)^{0.1} \tag{10}$$

μ_{G} = dynamic viscosity of water vapor.
When $1/X_{\mathrm{tt}} \leq 0.1$, F is equal to 1.
Chen boiling suppression factor:

$$S = \frac{1}{1 + 0.00000253\, Re_{\mathrm{tp}}^{1.17}} \tag{11}$$

Two-phase Reynolds number is given by:

$$Re_{\mathrm{tp}} = Re_{\mathrm{L}}F^{1.25} \tag{12}$$

Two-phase heat transfer coefficient obtained experimentally shows a good agreement with Chen correlation with an average deviation of ± 14%, refer Fig. 5.

Results and discussion

In this section, experimental results obtained for DI water and four different concentrations of Al_2O_3 and TiO_2 nanofluids have been discussed. Each nanofluid was evaluated for volumetric concentrations of 0.05%, 0.10%, 0.15% and 0.20% of nanoparticles. Mass flux was varied from 338 to 1014 kg m^{-2} s^{-1}, and heat flux was varied from 6.25 to 143.2 kW m^{-2}.

Effect of mass flux on the heat transfer coefficient

Results obtained from the experiments show that mass flux has a major influence on the thermal performance of flow boiling through an annulus. It was observed that the heat transfer coefficient increases with an increase in mass flux, refer Figs. 6–11. This is so because with the increase in the mass flux nucleation phenomena in boiling region decreases leading to a decrease in the average size of the bubbles. At higher mass flux, the time required for the bubble growth reduces significantly, and bubble diameter reduces. Smaller bubbles leave the surface quickly and transfer a good amount of heat to the fluid, which results in a higher rate of heat transfer.

It can also be seen in Figs. 6–11 that the heat transfer coefficient for water and the two nanofluids increases considerably with the increase in the heat flux. Heat transfer coefficient of water and the two nanofluids

increases more rapidly in the nucleate boiling region than in the forced convective region.

In the present study, the concentration of the nanoparticles in the base fluid was kept below 1%. A significant increase in the heat transfer coefficient was observed with the increase in the concentration of the nanoparticles in the base fluid. From the literature [1], it was seen that the heat transfer coefficient increases with the concentration of the nanoparticles in the base fluid up to a certain limit (normally 1%). After crossing this limit, a significant decrease in HTC is seen in the forced convective region and nucleate boiling region. At higher concentration of nanoparticles, the HTC deteriorates due to deposition and formation of the sludge of nanoparticles on the heating surface, which changes the wettability of the surface.

Figures 6–11 show the thermal performance of DI water and Al_2O_3 and TiO_2 nanofluids. From the figures, it can be stated that both the nanofluids show better thermal performance than DI water for every concentration as the thermo-physical properties of nanofluids are better than DI water. When a comparison is made between Al_2O_3 and TiO_2 nanofluids, Al_2O_3 shows better thermal performance than TiO_2 nanofluids because thermo-physical properties of Al_2O_3 nanofluid are better than TiO_2 nanofluid.

At a heat flux of 6.25 kW m^{-2}, mass flux of 338 kg m^{-2} s^{-1} and volumetric concentration of 0.20%, increase in the HTC of TiO_2 nanofluid as compared to that of water is 38.55% and at a mass flux of 1014 kg m^{-2} s^{-1} increase in the HTC of TiO_2 nanofluid as compared to that of water is 50.97%. When heat flux is raised to its highest value of 143.2 kW m^{-2}, the increase in HTC is 59.80% and 71.56% for the mass flux of 338 kg m^{-2} s^{-1} and 1014 kg m^{-2} s^{-1}, respectively.
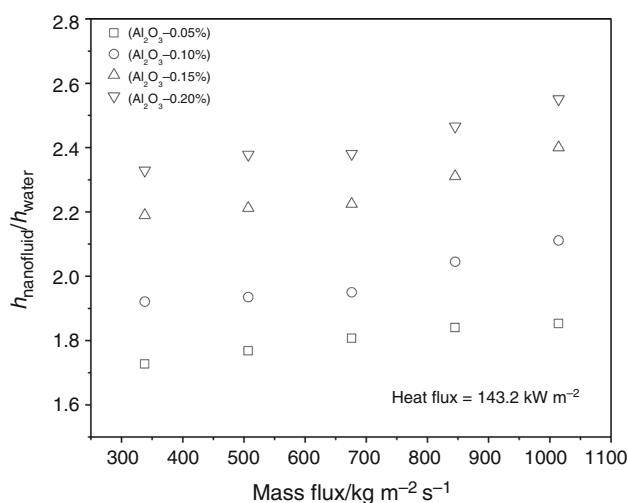

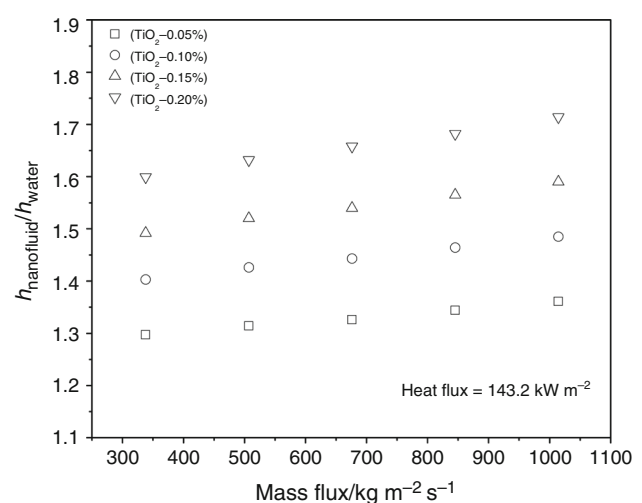Fig. 18 Flow boiling HTC ratios of Al_2O_3 nanofluid with mass flux at a heat flux of 143.2 kW m^{-2}

Fig. 19 Flow boiling HTC ratios of TiO_2 nanofluid with mass flux at a heat flux of 143.2 kW m^{-2}

Table 6 HTC ratio of Al$_2$O$_3$ nanofluid for heat flux (6.25–143.2) kW m^{-2}, mass flux (338–1014) kg m^{-2} s^{-1} and concentration (0.05–0.20%)

Al$_2$O$_3$ nanofluid at pressure = 1 bar

Mass flux/kg m^{-2} s^{-1}	HTC (Water)/kW m^{-2} K^{-1}	HTC (Al$_2$O$_3$ Nanofluid)/kW m^{-2} K^{-1}				$h_{nanofluid}/h_{water}$			
		Concentration				Concentration			
		0.05	0.10	0.15	0.20	0.05	0.10	0.15	0.20
Heat flux = 6.25 kW m^{-2}									
338.13	4.54	7.29	7.81	8.30	8.82	1.606	1.720	1.828	1.943
507.20	7.25	11.81	12.62	13.43	14.29	1.629	1.741	1.852	1.971
676.27	9.49	15.62	16.97	18.06	19.32	1.646	1.788	1.903	2.036
845.33	12.03	19.94	22.39	23.85	25.52	1.658	1.861	1.983	2.121
1014.40	14.77	25.08	28.33	30.02	31.93	1.698	1.918	2.032	2.162
Heat flux = 26.04 kW m^{-2}									
338.13	4.71	7.63	8.21	9.25	9.85	1.620	1.743	1.964	2.091
507.20	7.30	12.14	12.85	14.56	15.54	1.663	1.760	1.995	2.129
676.27	9.54	15.99	17.16	19.51	20.97	1.676	1.799	2.045	2.198
845.33	12.50	21.18	23.66	26.92	28.69	1.694	1.893	2.154	2.295
1014.40	16.13	27.84	31.20	35.48	37.82	1.726	1.934	2.200	2.345
Heat flux = 54.69 kW m^{-2}									
338.13	4.90	7.99	8.75	9.88	10.54	1.631	1.786	2.016	2.151
507.20	7.85	13.24	14.18	15.96	17.00	1.687	1.806	2.033	2.166
676.27	11.26	19.28	20.63	23.25	24.86	1.712	1.832	2.065	2.208
845.33	14.46	24.93	28.05	31.89	34.20	1.724	1.940	2.205	2.365
1014.40	16.95	29.45	33.53	37.96	40.39	1.737	1.978	2.240	2.383
Heat flux = 93.75 kW m^{-2}									
338.13	4.99	8.28	9.12	10.39	11.12	1.659	1.828	2.082	2.228
507.20	7.98	13.62	14.75	16.74	17.97	1.707	1.848	2.098	2.252
676.27	12.67	21.94	23.71	26.86	28.67	1.732	1.871	2.120	2.263
845.33	16.55	28.83	32.60	36.80	39.39	1.742	1.970	2.224	2.380
1014.40	17.55	30.73	35.10	39.73	42.44	1.751	2.000	2.264	2.418
Heat flux = 130.21 kW m^{-2}									
338.13	5.08	8.60	9.51	10.84	11.50	1.693	1.872	2.134	2.264
507.20	8.76	15.19	16.57	18.88	20.18	1.734	1.892	2.155	2.304
676.27	16.27	28.85	31.19	35.36	37.61	1.773	1.917	2.173	2.312
845.33	18.03	32.32	36.00	40.90	43.67	1.793	1.997	2.268	2.422
1014.40	24.02	43.38	49.77	56.54	60.04	1.806	2.072	2.354	2.500
Heat flux = 143.23 kW m^{-2}									
338.13	5.16	8.91	9.91	11.30	12.02	1.727	1.921	2.190	2.329
507.20	8.81	15.58	17.05	19.49	20.95	1.768	1.935	2.212	2.378
676.27	17.43	31.49	33.99	38.78	41.50	1.807	1.950	2.225	2.381
845.33	19.80	36.43	40.50	45.75	48.83	1.840	2.045	2.311	2.466
1014.40	26.83	49.72	56.65	64.39	68.44	1.853	2.111	2.400	2.551

Similarly, for Al$_2$O$_3$ nanofluid at a heat flux of 6.25 kW m^{-2}, mass flux of 338 kg m^{-2} s^{-1} and volumetric concentration of 0.20%, the increase in HTC of Al$_2$O$_3$ nanofluid as compared to that of water is 94.31% and at a mass flux of 1014 kg m^{-2} s^{-1}, increase in HTC of Al$_2$O$_3$ nanofluid as compared to that of water is 116.20%.

At a heat flux of 143.2 kW m^{-2}, the increase in HTC of Al$_2$O$_3$ nanofluid as compared to that of water is 132.64% and 155.24% for a mass flux of 338 kg m^{-2} s^{-1} and 1014 kg m^{-2} s^{-1}, respectively.

Table 7 HTC ratio of TiO_2 nanofluid for heat flux (6.25–143.2) kW m^{-2}, mass flux (338–1014) kg m^{-2} s^{-1} and concentration (0.05–0.20%)

TiO_2 nanofluid at pressure = 1 bar

Mass flux/kg m^{-2} s^{-1}	HTC (Water)/kW m^{-2} K^{-1}	HTC (TiO_2 Nanofluid)/kW m^{-2} K^{-1}				$h_{nanofluid}/h_{water}$			
		Concentration				Concentration			
		0.05	0.10	0.15	0.20	0.05	0.10	0.15	0.20
Heat flux = 6.25 kW m^{-2}									
338.13	4.54	5.59	5.83	6.06	6.29	1.231	1.284	1.335	1.385
507.20	7.25	9.01	9.39	9.79	10.23	1.243	1.295	1.350	1.411
676.27	9.49	11.89	12.52	13.10	13.67	1.253	1.319	1.380	1.440
845.33	12.03	15.15	16.15	17.00	17.83	1.259	1.342	1.413	1.482
1014.40	14.77	18.97	20.17	21.17	22.30	1.284	1.366	1.433	1.510
Heat flux = 26.04 kW m^{-2}									
338.13	4.71	5.84	6.19	6.48	6.82	1.240	1.314	1.376	1.448
507.20	7.30	9.17	9.76	10.26	10.94	1.256	1.337	1.405	1.499
676.27	9.54	12.07	12.95	13.65	14.45	1.265	1.357	1.431	1.515
845.33	12.50	15.98	17.21	18.15	19.51	1.278	1.377	1.452	1.561
1014.40	16.13	20.91	22.51	23.74	25.84	1.296	1.396	1.472	1.602
Heat flux = 54.69 kW m^{-2}									
338.13	4.90	6.11	6.57	6.89	7.35	1.247	1.341	1.406	1.500
507.20	7.85	9.94	10.71	11.29	12.02	1.266	1.364	1.438	1.531
676.27	11.26	14.35	15.58	16.45	17.52	1.274	1.384	1.461	1.556
845.33	14.46	18.66	20.33	21.55	23.09	1.290	1.406	1.490	1.597
1014.40	16.95	22.13	24.22	25.75	27.83	1.306	1.429	1.519	1.642
Heat flux = 93.75 kW m^{-2}									
338.13	4.99	6.29	6.79	7.22	7.65	1.261	1.361	1.447	1.533
507.20	7.98	10.19	11.05	11.77	12.48	1.277	1.385	1.475	1.564
676.27	12.67	16.27	17.78	18.97	20.23	1.284	1.403	1.497	1.597
845.33	16.55	21.52	23.59	25.15	27.14	1.300	1.425	1.520	1.640
1014.40	17.55	23.10	25.38	27.03	29.23	1.316	1.446	1.540	1.666
Heat flux = 130.21 kW m^{-2}									
338.13	5.08	6.48	7.01	7.46	7.93	1.276	1.380	1.469	1.561
507.20	8.76	11.28	12.31	13.08	13.88	1.288	1.405	1.493	1.584
676.27	16.27	21.15	23.18	24.77	26.39	1.300	1.425	1.522	1.622
845.33	18.03	23.76	26.05	27.99	30.24	1.318	1.445	1.552	1.677
1014.40	24.02	32.06	35.15	37.85	40.98	1.335	1.463	1.576	1.706
Heat flux = 143.23 kW m^{-2}									
338.13	5.16	6.69	7.24	7.70	8.25	1.297	1.403	1.492	1.599
507.20	8.81	11.58	12.56	13.39	14.38	1.314	1.426	1.520	1.632
676.27	17.43	23.11	25.16	26.85	28.90	1.326	1.443	1.540	1.658
845.33	19.80	26.62	28.99	30.98	33.30	1.344	1.464	1.565	1.682
1014.40	26.83	36.51	39.84	42.67	46.00	1.361	1.485	1.590	1.714

Effect of heat flux on the heat transfer coefficient

Variation in boiling HTC with heat flux for different mass fluxes is shown in Figs. 12–16. The figures show that the boiling heat transfer coefficient for all the mass fluxes increases with the increase in the heat flux. Higher rate of heat transfer is due to the bubble formation phenomena. Increases in HTC are more in the nucleate boiling region as compared to forced convection region which agrees with the results reported in the literature [20].
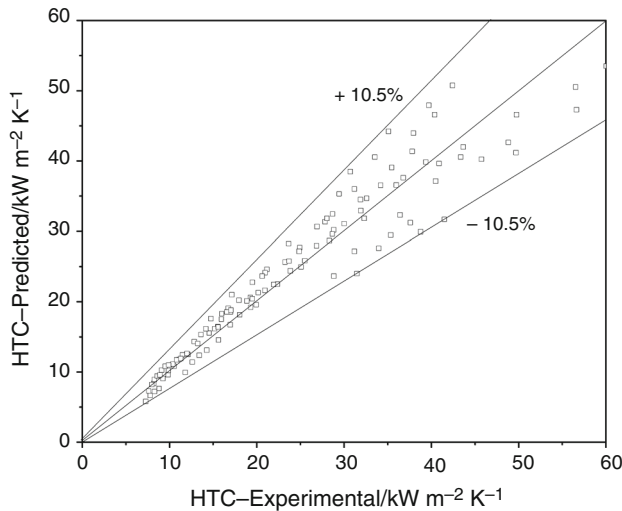
Fig. 20 Predicted values of HTC given correlation (Eq. 14) versus experimental values of HTC for Al$_2$O$_3$ nanofluid
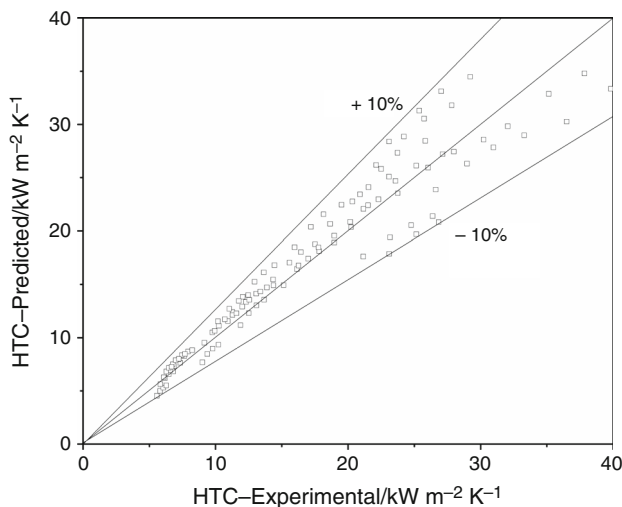

Fig. 21 Predicted values of HTC given correlation (Eq. 15) versus experimental values of HTC for TiO$_2$ nanofluid

With higher mass flux and higher heat flux, the turbulence intensity becomes higher due to an increase in the collision among the particles which results in the enhancement of heat transfer rate. This can be seen in Figs. 12–16, i.e., HTC also increases with the increase in the mass flux. HTC increase is seen more in nanofluids than that in water because rewetting occurs faster in nanofluids as compared to that in water.

Figures 12–16 show that HTC of Al$_2$O$_3$ and TiO$_2$ nanofluids increase as the concentration of nanoparticles in the base fluid increases. The Al$_2$O$_3$ nanofluid shows more increase in HTC as compared to TiO$_2$ nanofluid. This is so because the thermal conductivity of Al$_2$O$_3$ nanofluid is better than TiO$_2$ nanofluid.

The increase in HTC of TiO$_2$ nanofluid as compared to that of water, at a mass flux of 507 kg m^{-2} s^{-1}, heat flux of 26 kW m^{-2} and volumetric concentration of 0.05%, is 25.60% and at a heat flux of 130.2 kW m^{-2}, the increase in HTC of TiO$_2$ nanofluid as compared to that of water is 28.70%. When mass flux is raised to 845 kg m^{-2} s^{-1}, the increase in HTC of TiO$_2$ nanofluid as compared to that of water is 27.85% and 31.85% for a heat flux of 26 kW m^{-2} and 130.2 kW m^{-2}, respectively.

Similarly, for Al$_2$O$_3$ nanofluid, at a mass flux of 507 kg m^{-2} s^{-1}, heat flux of 26 kW m^{-2} and volumetric concentration of 0.05%, the increase in HTC of Al$_2$O$_3$ nanofluid as compared to that of water is 66.21% and at a heat flux of 130.2 kW m^{-2}, the increase in HTC of Al$_2$O$_3$ nanofluid as compared to that of water is 73.30%. At a mass flux of 845 kg m^{-2} s^{-1}, the increase in HTC of Al$_2$O$_3$ nanofluid as compared to that of water is 69.45% and 79.26% for a heat flux of 26 kW m^{-2} and 130.2 kW m^{-2}, respectively.

Forced convection and onset of nucleate boiling (ONB) regions are shown in Fig. 17. HTC of water and nanofluids increases with the increase in heat flux. Figure 17 shows that the heat transfer rate is more in the nucleate boiling region than forced convection region due to the higher formation of bubbles in the nucleate boiling region. ONB was achieved at a heat flux of 93.75 kW m^{-2}.

Improvement in HTC ratio

Flow boiling HTC ratio is defined as the ratios of HTC of nanofluid to HTC of DI water.

$$\text{Ratio}_{\text{HTC}} = \frac{h_{\text{nanofluid}}}{h_{\text{water}}} \qquad (13)$$

HTC ratio was calculated for both Al$_2$O$_3$ and TiO$_2$ nanofluids. HTC ratio increases with the increase in mass flux from 338 to 1014 kg m^{-2} s^{-1} for both the nanofluids for volumetric concentration varying from 0.05 to 0.20%. Figures 18 and 19 show the flow boiling HTC ratios for Al$_2$O$_3$ and TiO$_2$ nanofluids for the highest heat flux of 143.2 kW m^{-2} and volumetric concentration varying from 0.05 to 0.20%. Tables 6 and 7 show HTC ratio for Al$_2$O$_3$ and TiO$_2$ nanofluids, respectively, for heat flux varying from 6.25 to 143.2 kW m^{-2}, mass flux varying from 338 to 1014 kg m^{-2} s^{-1} and volumetric concentration varying from 0.05 to 0.20%. From the results, it is observed that HTC ratio increases for Al$_2$O$_3$ and TiO$_2$ nanofluids with an increase in mass flux, heat flux and volumetric concentration. But HTC ratio of Al$_2$O$_3$ nanofluid is higher than TiO$_2$ nanofluids, as the thermal conductivity of Al$_2$O$_3$ is higher than TiO$_2$ nanofluids.

At high mass flux, the ratio of heat transfer coefficient of nanofluid to water increases significantly because high

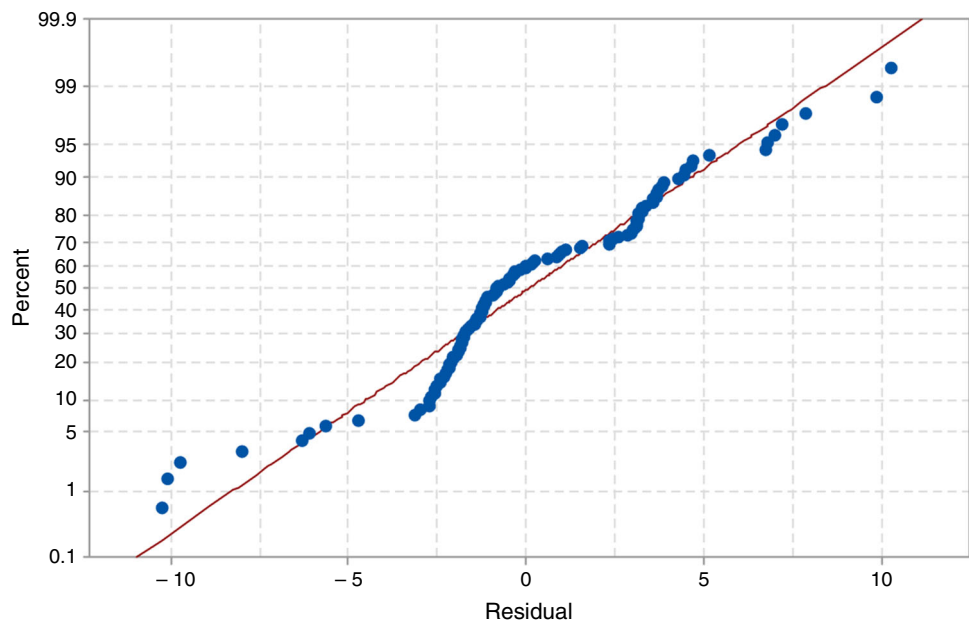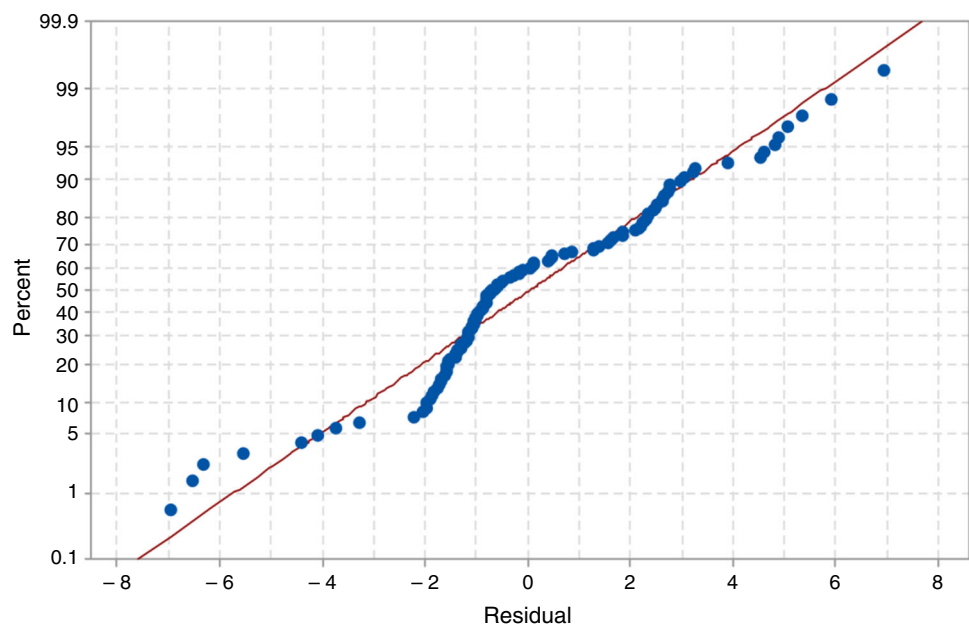**Fig. 22** Normal probability plot of HTC correlation of Al_2O_3 nanofluid

Fig. 23 Normal probability plot of HTC correlation of TiO_2 nanofluid

mass flux accelerates heat transfer from the heated surface. At high mass flux, diameter of the bubbles reduces and lower diameter bubbles detach from the heated surface rapidly and a fair quantity of heat is transferred to the fluid leading to the increase in HTC ratio.

Correlations development for HTC

Based on the present study, two different correlations for HTC for flow boiling in Al_2O_3 and TiO_2 nanofluids have been developed using 120 data points. HTC of nanofluids has been expressed as a function of mass flux, volumetric concentration of nanoparticles, and heat flux. In Figs. 20 and 21, experimental values of HTC have been compared with predicted values of HTC which are calculated through correlations. As shown, the predicted HTC values are in good agreement with the experimental data. Value of correlation coefficient R^2 is determined for both the correlations. In case of Al_2O_3, the value of R^2 is 96.94% and the mean deviation of the predicted HTC from the experimental HTC is $\pm$ 10.5% whereas in case of TiO_2 the value of R^2 is 96.96% and the mean deviation of the predicted HTC from the experimental HTC is $\pm$ 10%. The

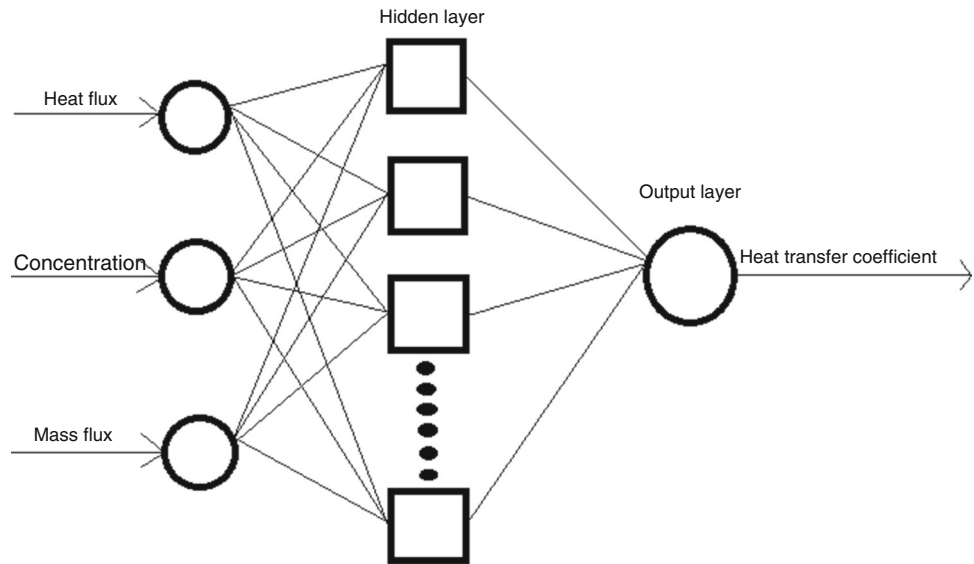**Fig. 24** ANN structure used in the current study

Table 8 MSE and R values for response h (heat transfer coefficient) for Al$_2$O$_3$ nanofluid

	Samples	MSE	R
Training	84	0.144532	0.999612
Validation	18	0.852950	0.998059
Testing	18	0.829852	0.997671

Table 9 MSE and R values for response h (heat transfer coefficient) for TiO$_2$ nanofluid

	Samples	MSE	R
Training	84	0.081670	0.999527
Validation	18	0.167398	0.999153
Testing	18	0.264380	0.998722

Fig. 25 Comparison of HTC from experiment and ANN for Al$_2$O$_3$ nanofluid

developed correlations of HTC of Al$_2$O$_3$ and TiO$_2$ are given below:

$$h_{\text{Al}_2\text{O}_3} = 0.0034 \times (q)^{0.16} \times (C)^{0.20} \times (G)^{1.33} \qquad (14)$$

$$h_{\text{TiO}_2} = 0.0027 \times (q)^{0.15} \times (C)^{0.14} \times (G)^{1.30} \qquad (15)$$

where q = heat flux, kW m^{-2}, C = concentration of nanofluids by volume, G = mass flux, kg m^{-2} s^{-1}.

Normal probability plots of HTC correlation of Al$_2$O$_3$ and TiO$_2$ nanofluids are shown in Figs. 22 and 23. In a normal probability, nearly a straight diagonal line is formed by the data points which shows normally distributed data. As shown in Figs. 22 and 23, many of the data points are very near to residual value zero in both the cases and correlation coefficients have the values near to unity which indicates minimum errors in developed correlations.
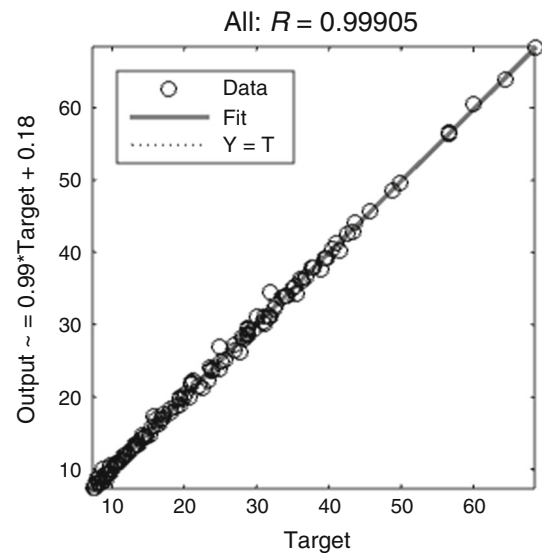
Artificial neural network modeling

ANN is a computational tool comprising of many simple and highly interconnected processing elements. By using its dynamic system response to external inputs, ANN approach has the capability to study highly nonlinear relationships and complete information of the process [32]. ANN model is developed to predict the heat transfer coefficients of both Al$_2$O$_3$ and TiO$_2$ nanofluids in the current study. For prediction in mechanical engineering
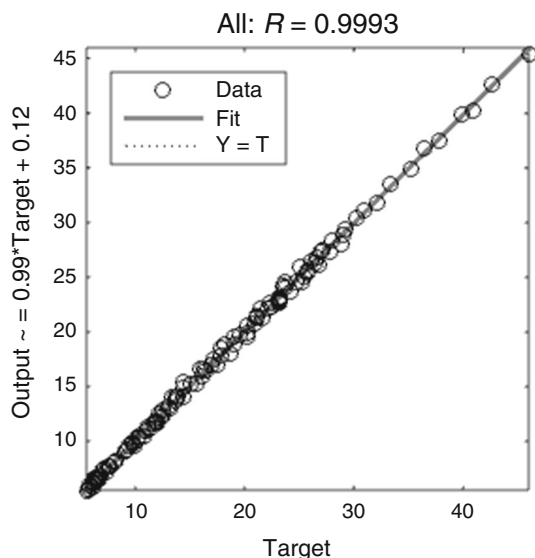
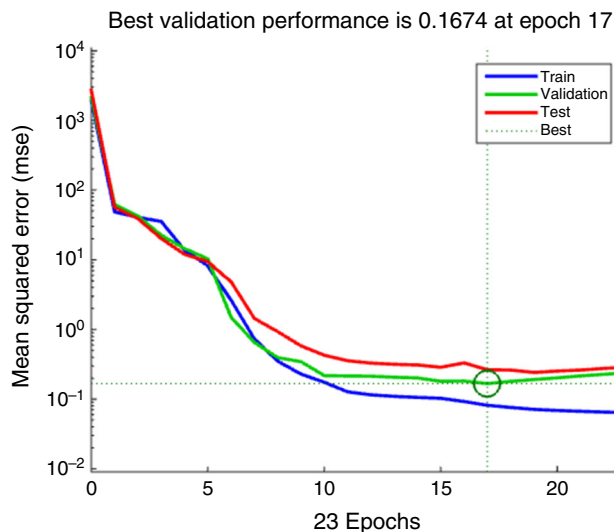Fig. 26 Comparison of HTC from experiment and ANN for TiO$_2$ nanofluid

Fig. 28 Variation of MSE with epochs for optimal ANN model for TiO$_2$ nanofluid
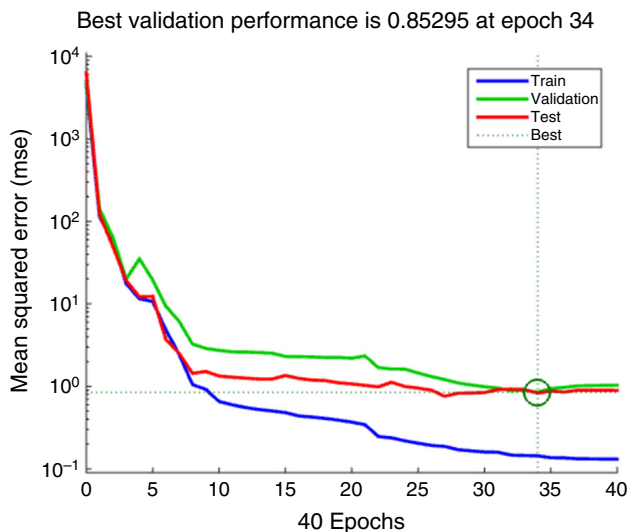

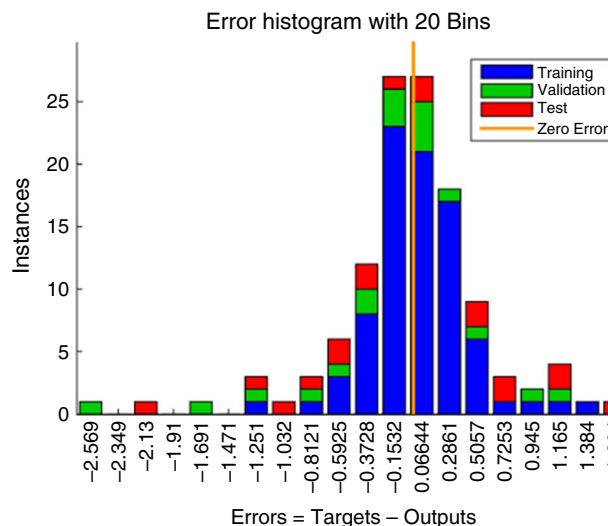Fig. 27 Variation of MSE with epochs for optimal ANN model for Al$_2$O$_3$ nanofluid

Fig. 29 Error histogram with 20 bins for the training, validation and test steps for Al$_2$O$_3$ nanofluid

application, the most common method used is multilayer perceptron, which is a feed-forward ANN containing input and output layers, and at least one layer of processing units between input and output layers called hidden layer. Figure 24 shows the schematic diagram of the ANN model used in this study. MATLAB was used for ANN designing.

Following steps were followed for designing experimentation and data collection; data analysis and preprocessing; ANN designing; ANNs training and testing; simulation and prediction with ANNs; and analysis and post-processing of the predicted result. The algorithm used for network training is Levenberg–Marquardt [33]. The network consists of an input layer with three neurons (heat

flux, volumetric concentration and mass flux) an output layer of one neuron (heat transfer coefficient "h"), and a hidden layer of ten neurons. Tables 8 and 9 show MSE and R values for response h (heat transfer coefficient) for Al$_2$O$_3$ and TiO$_2$ nanofluid, respectively.

Figures 25 and 26 show the comparison between the values of heat transfer coefficient obtained from the optimal ANN model and experimental data set for Al$_2$O$_3$ and TiO$_2$ nanofluid, respectively. In both figures, the target value is the experimental heat transfer coefficient and the output value is predicted heat transfer coefficient. The optimal ANN model gives $R = 0.99905$ for Al$_2$O$_3$ nanofluid and $R = 0.9993$ for TiO$_2$ nanofluid between the predicted heat transfer coefficient and the experimental heat
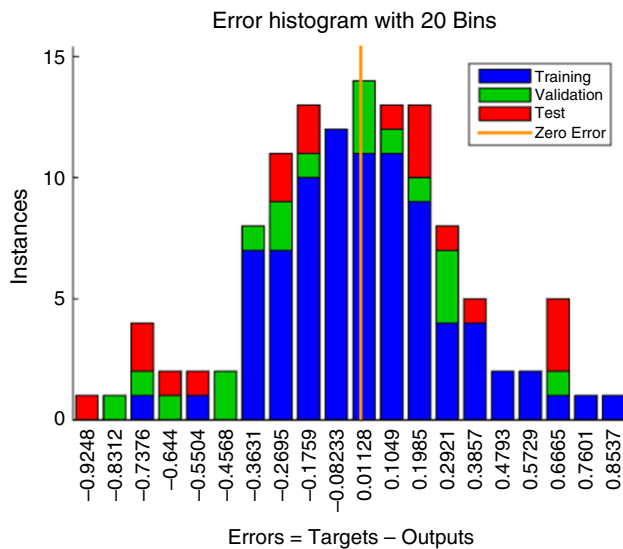
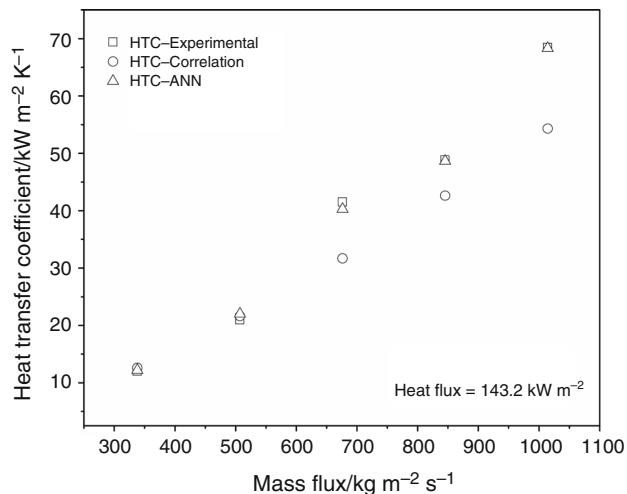**Fig. 30** Error histogram with 20 bins for the training, validation and test steps for TiO$_2$ nanofluid

Fig. 31 Comparison between experimental, correlation and ANN heat transfer coefficient of Al$_2$O$_3$ nanofluid along with mass flux at a heat flux of 143.2 kW m^{-2}

transfer coefficient. The comparison between the experimental results and ANN results are in good agreement.

As shown in Figs. 27 and 28, MSE against epochs during the training process of the optimum network are plotted for Al$_2$O$_3$ and TiO$_2$ nanofluid, respectively. The best results for Al$_2$O$_3$ nanofluid are achieved in 34 epoch with minimum MSE of 0.85295, whereas in case of TiO$_2$ nanofluid it is achieved in 17 epoch with minimum MSE of 0.1674 for validation of data set.

Figures 29 and 30 show error histogram with 20 bins for three steps, i.e., training, validation and test in artificial neural network modeling for Al$_2$O$_3$ and TiO$_2$ nanofluids, respectively. As shown in the figures, the zero error is illustrated with an orange line in the middle. It can be seen
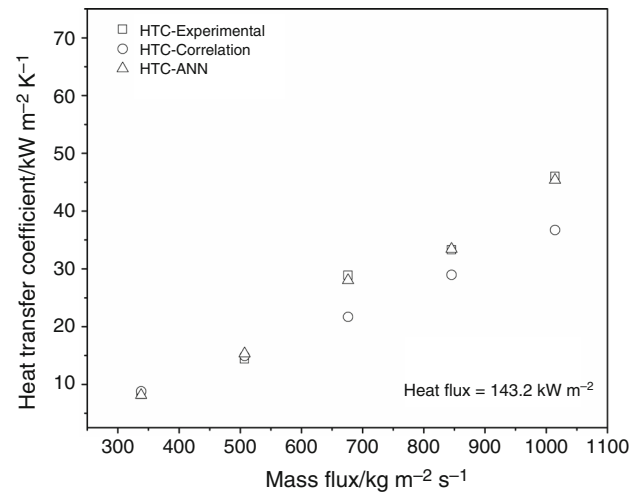

Fig. 32 Comparison between experimental, correlation and ANN heat transfer coefficient of TiO$_2$ nanofluid along with mass flux at a heat flux of 143.2 kW m^{-2}

in the histogram that most of the data points are closer to zero error line which means the error is less in ANN nonlinear prediction modeling for both Al$_2$O$_3$ and TiO$_2$ nanofluids. But when the comparison is made between Al$_2$O$_3$ and TiO$_2$ nanofluids, Al$_2$O$_3$ nanofluid shows better results than TiO$_2$ nanofluid as more data points are closer to zero error line.

Figures 31 and 32 show heat transfer coefficient obtained from experiments, correlations and ANN for Al$_2$O$_3$ nanofluid and TiO$_2$ nanofluid, respectively. Results predicted by ANN and correlations are in good agreement with the experimental results for both the nanofluids. However, ANN results are in better agreement with the experimental results than the results obtained by correlations. This is evident in Figs. 31 and 32.

Conclusions

In the present study, improvement in heat transfer for flow boiling for water-based Al$_2$O$_3$ and TiO$_2$ nanofluids with respect to DI water has been examined for varying heat flux, mass flux and concentrations. Following observations have been made:

- Heat transfer coefficient for DI water obtained from Chen correlation and experiments are in good agreement with the average deviation of ± 14%.
- With the increase in heat flux, concentration and mass flux, heat transfer coefficient for Al$_2$O$_3$ and TiO$_2$ nanofluid increases considerably. At highest heat flux of 143.2 kW m^{-2}, highest mass flux of 1014 kg m^{-2} s^{-1} and highest volumetric concentration of 0.20%, heat transfer coefficient of Al$_2$O$_3$ nanofluid increases by

155.24% as compared to that for the base fluid (water) and for TiO_2 nanofluid heat transfer coefficient increases by 71.56% as compared to that for the base fluid (water).

- Flow boiling HTC ratios, i.e., the ratios of HTC of nanofluid to HTC of DI water, increases with an increase in heat flux, volumetric concentration and mass flux. At highest heat flux of 143.2 kW m^{-2}, the highest mass flux of 1014 kg m^{-2} s^{-1} and highest volumetric concentration of 0.20%, HTC ratio for Al_2O_3 nanofluid is 2.551 and for TiO_2 it is 1.714.

- Heat transfer coefficient and HTC ratio for Al_2O_3 nanofluid are considerably higher than that for TiO_2 nanofluid. This is so because the thermo-physical properties of Al_2O_3 nanofluid and particularly its thermal conductivity are better than TiO_2 nanofluid. Some other factors like nucleation site density, contact angle, etc., are also responsible for the increase in HTC.

- Nonlinear correlations were developed for the heat transfer coefficient for Al_2O_3 and TiO_2 nanofluids based on heat flux, mass flux and volumetric concentration. The mean deviations between HTC values predicted by the correlations and the experimental values were $\pm 10.5\%$ and $\pm 10\%$ for Al_2O_3 and TiO_2 nanofluids, respectively.

- ANN model was developed to predict the heat transfer coefficient for flow boiling of nanofluids. Predicted values from ANN models were compared with the experimental values and the values obtained from the correlations. Results predicted by ANN are in better agreement with the experimental results as compared to the results predicted by the correlations.

References

1. Azmi WH, Sharma KV, Sarma PK, Mamat R, Anuar S. Comparison of convective heat transfer coefficient and friction factor of TiO_2 nanofluid flow in a tube with twisted tape inserts. Int J Therm Sci. 2014;81(1):84–93.
2. Zhou J, et al. Saturated flow boiling heat transfer investigation for nanofluid in minichannel. Exp Therm Fluid Sci. 2017;85:189–200.
3. Il Kim T, Jeong YH, Chang SH. An experimental study on CHF enhancement in flow boiling using Al_2O_3 nano-fluid. Int J Heat Mass Transf. 2010;53(5–6):1015–22.
4. Ahn HS, Kim H, Jo HJ, Kang SH, Chang WP, Kim MH. Experimental study of critical heat flux enhancement during forced convective flow boiling of nanofluid on a short heated surface. Int J Multiph Flow. 2010;36(5):375–84.
5. Kahani M, Zeinali Heris S, Mousavi SM. Comparative study between metal oxide nanopowders on thermal characteristics of nanofluid flow through helical coils. Powder Technol. 2013;246:82–92.
6. Şendur K, Pınar Mengüç M, Karimzadehkhouei M, Koşar A, Yalcin SE. Pressure drop and heat transfer characteristics of nanofluids in horizontal microtubes under thermally developing flow conditions. Exp Therm Fluid Sci. 2014;67:37–47.
7. Kim SJ, McKrell T, Buongiorno J, Wen Hu L. Subcooled flow boiling heat transfer of dilute alumina, zinc oxide, and diamond nanofluids at atmospheric pressure. Nucl Eng Des. 2010;240(5):1186–94.
8. Il Kim T, Chang WJ, Chang SH. Flow boiling CHF enhancement using Al_2O_3 nanofluid and an Al_2O_3 nanoparticle deposited tube. Int J Heat Mass Transf. 2011;54(9–10):2021–5.
9. Abedini E, Behzadmehr A, Rajabnia H, Sarvari SMH, Mansouri SH. Experimental investigation and comparison of subcooled flow boiling of TiO_2 nanofluid in a vertical and horizontal tube. Proc Inst Mech Eng Part C J Mech Eng Sci. 2013;227(8):1742–53.
10. Hasheminia M, Fard MH, Etemad SG, Hasan S. Forced boiling of nanofluids, effects of contact angle and surface wettability. In: 3rd micro and nano flows conference, 2011, no. August, p. 22–24.
11. Prajapati OS, Rohatgi N. Flow boiling heat transfer enhancement by using ZnO-water nanofluids. Sci Technol Nucl Install. 2014;2014:1–7.
12. Zeitoun O, Ali M. Nanofluid impingement jet heat transfer. Nanoscale Res Lett. 2012;7:1–14.
13. Qi C, Wan Y-L, Li C-Y, Han D-T, Rao Z-H. Experimental and numerical research on the flow and heat transfer characteristics of TiO_2-water nanofluids in a corrugated tube. Int J Heat Mass Transf. 2017;115:1072–84.
14. Abdollahi A, Mohammed HA, Vanaki SM, Osia A, Golbahar Haghighi MR. Fluid flow and heat transfer of nanofluids in microchannel heat sink with V-type inlet/outlet arrangement. Alex Eng J. 2017;56(1):161–70.
15. Wang Y, Su GH. Experimental investigation on nanofluid flow boiling heat transfer in a vertical tube under different pressure conditions. Exp Therm Fluid Sci. 2016;77:116–23.
16. Mohammed HI, Giddings D, Walker GS. Experimental investigation of nanoparticles concentration, boiler temperature and flow rate on flow boiling of zinc bromide and acetone solution in a rectangular duct. Int J Heat Mass Transf. 2019;130:710–21.
17. Sarafraz MM, Arya H, Saeedi M, Ahmadi D. Flow boiling heat transfer to MgO-therminol 66 heat transfer fluid: experimental assessment and correlation development. Appl Therm Eng. 2018;138(January):552–62.
18. Moreira TA, do Nascimento FJ, Ribatski G. An investigation of the effect of nanoparticle composition and dimension on the heat transfer coefficient during flow boiling of aqueous nanofluids in small diameter channels (1.1 mm). Exp Therm Fluid Sci. 2017;89(July):72–89.
19. Kamel MS, Lezsovits F, Hussein AK. Experimental studies of flow boiling heat transfer by using nanofluids. J Therm Anal Calorim. 2019;2:123.
20. Sarafraz MM, Hormozi F. Scale formation and subcooled flow boiling heat transfer of CuO-water nanofluid inside the vertical annulus. Exp Therm Fluid Sci. 2014;52:205–14.
21. Rana KB, Agrawal GD, Mathur J, Puli U. Measurement of void fraction in flow boiling of ZnO-water nanofluids using image processing technique. Nucl Eng Des. 2014;270:217–26.
22. Edel Z, Mukherjee A. Flow boiling dynamics of water and nanofluids in a single microchannel at different heat fluxes. J Heat Transf. 2014;137(1):011501 (1–8).
23. Moreira TA, do Nascimento FJ, Ribatski G. Flow boiling heat transfer coefficient of DI-water/SiO_2 nanofluid inside a 1.1 mm

round microchannel. In: Proceedings of the 13th international conference on nanochannels, microchannels, and minichannels, 2015, July, p. 1–6.

24. Duursma G, Wang Y, Harmand S, Sefiane K, Dehaene A. Flow and heat transfer of single-and two-phase boiling of nanofluids in microchannels. Heat Transf Eng. 2014;36(14–15):1252–65.

25. Xu L, Xu J. Nanofluid stabilizes and enhances convective boiling heat transfer in a single microchannel. Int J Heat Mass Transf. 2012;55(21–22):5673–86.

26. Chehade AA, Gualous HL, Le Masson S, Fardoun F, Besq A. Boiling local heat transfer enhancement in minichannels using nanofluids. Nanoscale Res Lett. 2013;8(1):1–20.

27. Sarafraz MM, Hormozi F. Forced convective and nucleate flow boiling heat transfer to alumina nanofluids. Period Polytech Chem Eng. 2014;58(1):37–46.

28. Paul G, Das PK, Manna I. Assessment of the process of boiling heat transfer during rewetting of a vertical tube bottom flooded by alumina nanofluid. Int J Heat Mass Transf. 2016;94:390–402.

29. Chen JC. Correlation for boiling heat transfer to saturated fluids in convective flow. Ind Eng Chem Des Dev. 1966;5(3):322–9.

30. Hussein AM, Sharma KV, Bakar RA, Kadirgama K. The effect of nanofluid volume concentration on heat transfer and friction factor inside a horizontal tube. J Nanomater. 2013;2013:1–12.

31. Moffat RJ. Describing the uncertainties in experimental results. Exp Therm Fluid Sci. 1988;1(1):3–17.

32. Jalili-kharaajoo M, Araabi BN. Neural network based predictive control of a heat exchanger non linear process. J Electr Electron Eng. 2004;4(2):1219–26.

33. Kamble LV, Pangavhane DR, Singh TP. Artificial neural network based prediction of heat transfer from horizontal tube bundles immersed in gas-solid fluidized bed of large particles. J Heat Transf. 2014;137(1):012901 (1–9).